THE JOURNAL OF PHYSICAL CHEMISTRY Letters

Letter

Cite This: J. Phys. Chem. Lett. 2018, 9, 7079−7084

pubs.acs.org/JPCL

Synthesis of All-Inorganic Cd-Doped $CsPbCl_3$ Perovskite Nanocrystals with Dual-Wavelength Emission

Tong Cai,[†] Hanjun Yang,[†] Katie Hills-Kimball,[†] Jeong-Pil Song,[†] Hua Zhu,[†] Elan Hofman,[‡] Weiwei Zheng,[‡] Brenda M. Rubenstein,[†] and Ou Chen*[,†]

[†]Department of Chemistry, Brown University, Providence, Rhode Island 02912, United States

[‡]Department of Chemistry, Syracuse University, Syracuse, New York 13244, United States

Supporting Information

ABSTRACT: Doped lead halide perovskite nanocrystals (NCs) have garnered significant attention due to their superior optoelectronic properties. Here, we report a synthesis of Cd-doped $CsPbCl_3$ NCs by decoupling Pb- and Cl-precursors in a hot injection method. The resulting Cd-doped perovskite NCs manifest a dual-wavelength emission profile with the first reported example of Cd-dopant emission. By controlling Cd-dopant concentration, the emission profile can be tuned with a dopant emission quantum yield of up to 8%. A new secondary emission (~610 nm) is induced by an energy transfer process from photoexcited hosts to Cd-dopants and a subsequent electronic transition from the excited state (^3E_g) to the ground state ($^1A_{1g}$) of $[CdCl_6]^{4-}$ units. This electronic transition matches well with a first-principles density functional theory calculation. Further, the optical behavior of Cd-doped $CsPbCl_3$ NCs can be altered through postsynthetic anion-exchange reactions. Our studies present a new model system for doping chemistry studies in semiconductors for various optoelectronic applications.

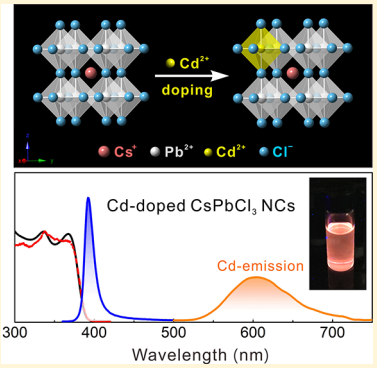

Lead halide perovskites ($APbX_3$; A = $CH_3NH_3^+$, Cs^+, etc.; X = Cl^-, Br^-, I^-) have recently garnered an immense amount of research interest because they offer the promise of revolutionizing optoelectronic applications such as solar cells,[1,2] lasers,[3,4] light-emitting diodes (LEDs),[5−9] photodetectors,[10] etc.[11−14] All-inorganic $CsPbX_3$ nanocrystals (NCs) have garnered an especially large amount of attention due to their superior optical properties and improved structural stability compared to these of organic−inorganic hybrid perovskites.[12−16] Since Protesescu et al. first reported the synthesis of high-quality colloidal $CsPbX_3$ nanocubes,[17] various synthetic protocols have been developed to obtain $CsPbX_3$ NCs with controlled sizes,[18,19] morphologies,[20−22] and tunable compositions.[23−25]

Doping metal ions into perovskite NCs can induce novel changes in their optical, electronic, and magnetic properties, opening a new research direction.[26,27] Especially when dopants with suitable electronic energy band alignment relative to the host perovskite NCs are used, new emission features can be introduced through a host-to-dopant energy transfer process. In particular, dual-emission perovskite NCs have been created via doping and found to be exceedingly useful in many applications, such as white light LEDs[28] and luminescent solar concentrators.[29] In this regard, multiple systems utilizing main group, transition, and rare earth elements as dopants have been reported to date.[30−39] For example, Mn^{2+} is arguably the most popular dopant because it can accept energy from photoexcited host perovskite NCs, resulting in a new emission peak (580−620 nm) through the d−d transition of the Mn-dopants.[40−46] As another well-studied example, Yb^{3+} trivalent dopants can lead to a dual-wavelength emission spanning both the visible and near-infrared spectral regions.[47−51] In this case, Yb^{3+}-dopants act as a luminescence activator involving energy relaxation from the excited state $^2F_{5/2}$ to the ground state $^2F_{7/2}$ and give rise to emission at ~990 nm with photoluminescence quantum yields (PL QYs) exceeding unity.[48]

Herein, we report a synthesis of Cd-doped $CsPbCl_3$ NCs through a hot injection method. The emergence of a new broad emission band centered at ~610 nm is observed and attributed to the Cd-dopant PL through an energy transfer process from the host $CsPbCl_3$ NCs to the Cd^{2+} ions. In addition, this facile synthetic approach allows us to study the variation of optical properties of $CsPbCl_3$ perovskite NCs with different doping concentrations. First-principles density functional theory (DFT) calculations reveal that the Cd-dopant emission is attributed to the energy relaxation process from the excited state (^3E_g) to the ground state ($^1A_{1g}$) of $[CdCl_6]^{4-}$ units. Lastly, we show that a Cl-to-Br anion-exchange can be employed to tune the optical properties of the Cd-doped NCs postsynthetically.

Our colloidal synthesis of Cd-doped $CsPbCl_3$ NCs builds upon a previously reported hot injection method,[52] where we introduce $Cd(CH_3COO)_2{\cdot}2H_2O$ (Cd-acetate) as a dopant precursor. In a typical synthesis, Cs_2CO_3, $Pb(CH_3COO)_2{\cdot}$

Received: November 9, 2018
Accepted: December 3, 2018
Published: December 4, 2018

DOI: 10.1021/acs.jpclett.8b03412
J. Phys. Chem. Lett. 2018, 9, 7079−7084

$3H_2O$ (Pb-acetate), and Cd-acetate were added to a mixture of oleic acid, oleylamine, and 1-octadecene, and the resulting solution was heated under vacuum. At 200 °C, benzoyl chloride was swiftly injected into the flask, triggering NC formation (see the SI for details). Compared to the conventional approach, in which $PbCl_2$ was commonly used as the source of both Pb and Cl, in our synthesis, metal acetates (i.e., Pb-acetate and Cd-acetate) were used as the distinct Pb and Cd sources, and benzoyl chloride was used as the sole Cl source to eliminate pre-existing Pb−Cl bonds prior to NC formation. In this case, simultaneous incorporation of Pb^{2+} and Cd^{2+} ions in the perovskite NCs was achieved due to fast and kinetically controlled NC nucleation and growth,[53] despite a large discrepancy in the bond dissociation energies between Pb−Cl (301 kJ/mol) and Cd−Cl (208 kJ/mol).[54] As a control experiment, doping Cd^{2+} ions in $CsPbCl_3$ NCs failed when replacing Pb-acetate with $PbCl_2$ as the single source for both Pb and Cl,[17,52] which strongly supports our hypothesis. In addition to enabling successful doping, this approach allows for facile tunability in the Cd-doping level by altering the stoichiometry of the Pb- and Cd-precursors fed into the reaction (discussed in detail below).

Figure 1A shows the scheme for doping a Cd^{2+} ion into the $CsPbCl_3$ perovskite crystal lattice. While the undoped $CsPbCl_3$ NCs manifested similar properties to those previously reported (Figure 1B,C),[17,52] the Cd-doped $CsPbCl_3$ NCs showed a new emission band at 610 nm (full width at half-maximum of 88 nm) with a maximal PL QY of ~8% (Figure 1D). The PL excitation (PLE) spectrum obtained from monitoring the emission at 610 nm matched well with the absorption profile, indicating that the emission band was a result of an energy transfer process from host NCs to Cd-dopants (Figure 1D). The bandgap (BG) emission peak of the Cd-doped NCs (Figure 1D) was blue-shifted with an enlarged Stokes shift compared to that of the undoped NCs (168 vs 96 meV) (Figure 1B,D). This is indicative of an alloying effect that is accompanied by lattice contraction upon introduction of Cd-dopants,[28,30] as well as a stronger quantum confinement effect as evidenced by the smaller particle size of the Cd-doped NCs than their undoped counterparts (8.8 ± 0.7 vs 10.2 ± 1.1 nm) (Figures 1C,E, S1, and S2). Due to the high morphological uniformities of both samples, the perovskite NCs can self-assemble into an ordered monolayer whose localized selected-area electron diffraction (SA-ED) signals indicate a cubic symmetry (Figure 1C,E, insets). Although Cd-doped $CsPbCl_3$ NCs have been synthesized through a postcation-exchange process,[30] Cd-dopant emission has not been observed previously, which is likely due to the surface and crystal defects induced by the cation-exchange reaction.

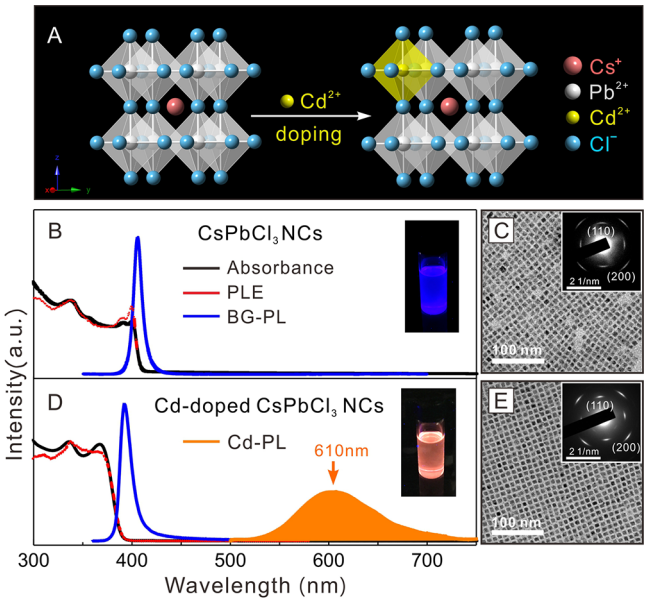

Figure 1. (A) Schematic of the Cd-dopant substitution in $CsPbCl_3$ unit cells. (B,D) Absorption (black), PL (blue, orange), and PLE (red) spectra of the undoped and Cd-doped $CsPbCl_3$ NCs. Insets: photographs of the sample under UV illumination (365 nm). (C,E) TEM images of the undoped and Cd-doped $CsPbCl_3$ NCs. Insets: SA-ED patterns.

To study how Cd-doping levels affect NC optical properties, different molar percentages of the Cd-precursor ([Cd]/([Cd] + [Pb])) were added during the synthesis (see the SI for details). The actual Cd-dopant concentrations were determined through elemental analysis using an inductively coupled plasma-atomic emission spectrometer. When adding 6, 10, 14, and 18% Cd-precursor, the corresponding Cd-doping concentrations in the final NCs were measured to be 2.26, 5.40, 9.28, and 11.49%, respectively (Table S1). The lower Cd-dopant percentages as compared to the synthesis feed ratio are a result of less than unity dopant reaction yields.[31,40,48] While there were no appreciable differences in the absorption spectra, the intensity ratios of the Cd-to-BG PL peaks monotonically increased as the Cd-doping concentration increased from 0 to 9.28%, at which it reached a maximum value of 0.36 (Figure 2A−C). Upon further increase of the Cd-doping concentration, the PL intensity ratio decreased (Figure 2A−C), which was likely caused by the presence of crystalline defects and an interdopant coupling-induced self-quenching effect due to the introduction of excess Cd-dopants.[28,40,48]

PL lifetime measurements showed that the average lifetime (τ_{BG}) of the BG-PL decreased dramatically from 8.43 to 2.33 ns when increasing the doping concentration from 0 to 11.49% (Figure 2D and Table S2). The trend was consistent with the increased doping concentration, which produced more photoactive acceptors inside of the host NCs.[48] This led to a faster energy transfer rate from the photoexcited $CsPbCl_3$ NCs to the Cd-dopants, thus accelerating depletion of the excitonic transitions.[30,48] However, the decay curves of the Cd-PL showed single-exponential behavior with similar fitted lifetime (τ_{Cd}) values of 1.32−1.35 ms for all doping concentrations (Figure 2E and Table S3). This minimal lifetime variance and single-exponential decay behavior across all samples suggest a uniform local lattice environment at the Cd-doping sites in the host lattice.[40,41]

TEM measurements showed that all of the Cd-doped NCs possessed a cubic shape with high morphological uniformity (Figures 3A−C and S3−S5). Upon increasing the Cd-doping concentration, the average edge length decreased from 9.8 ± 1.0 nm for the NCs with a doping concentration of 2.26% to 7.7 ± 0.9 nm for the 11.49% case. Powder X-ray diffraction (XRD) measurements revealed that all of the Cd-doped $CsPbCl_3$ NCs possessed a cubic perovskite phase (space group: $Pm\bar{3}m$), thus retaining the same as their undoped counterparts (Figure 3D). However, careful examination of the XRD patterns showed that the diffraction peaks were monotonically shifted to higher angles upon increasing the Cd-doping concentration, revealing a monotone lattice

DOI: 10.1021/acs.jpclett.8b03412
J. Phys. Chem. Lett. 2018, 9, 7079−7084

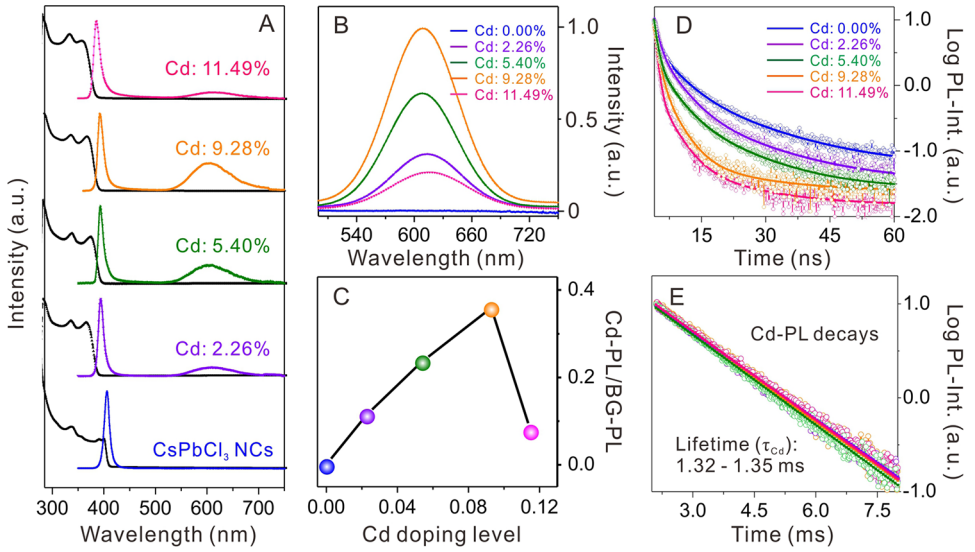

Figure 2. (A) UV−vis absorption (black lines) and PL spectra (colored lines, λ_{ex} = 340 nm) of the Cd-doped $CsPbCl_3$ NCs with different doping concentrations. (B) Zoomed-in Cd-PL spectra. (C) Intensity ratios of the Cd- to BG-PL as a function of Cd-doping concentration. Lifetime decay curves for (D) BG-PL with different Cd-doping concentrations and (E) Cd-PL of the sample with different Cd-doping concentrations.

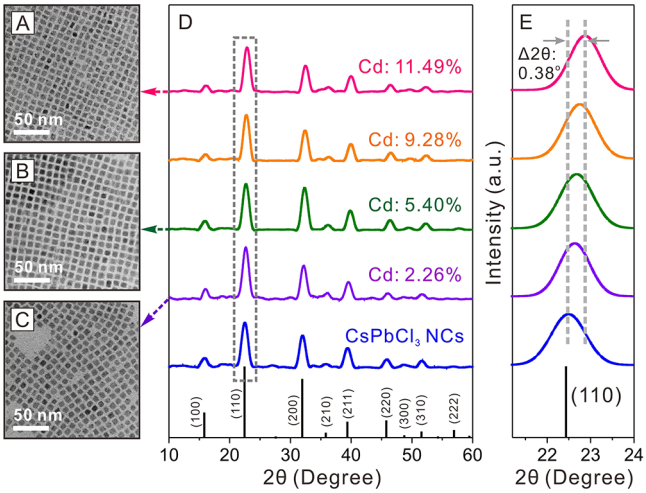

Figure 3. (A−C) TEM images and (D) XRD patterns of Cd-doped $CsPbCl_3$ NCs with different doping concentrations. (E) Zoomed-in XRD patterns of the (110) diffraction peak.

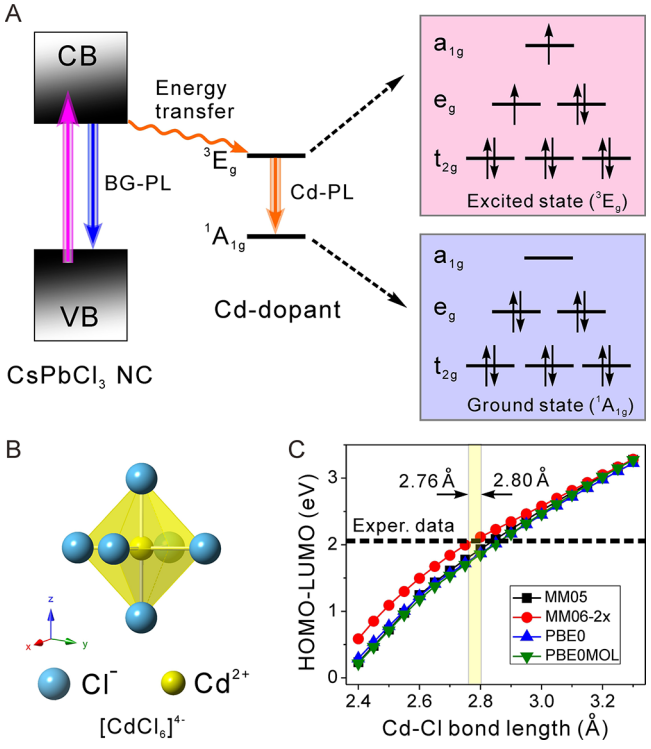

Figure 4. (A) Schematic of the energy transfer process from the host NC to Cd-dopant (left) and the corresponding ground/excited states of Cd-dopants (right). (B) Atomic model of the $[CdCl_6]^{4-}$ octahedral unit. (C) First-principles DFT calculation results for the HOMO−LUMO energy gaps for $[CdCl_6]^{4-}$ using different hybrid functionals.

contraction trend (Figure 3D,E). The calculated lattice constant decreased from 5.60 to 5.51 Å from undoped NCs to the NCs with 11.49% Cd-doping (Figures S6−S10 and Tables S4−S9). This lattice contraction was in line with the replacement of larger Pb^{2+} ions (ionic radius: 119 pm) with smaller Cd^{2+} ions (ionic radius: 95 pm),[30] suggesting successful incorporation of Cd-dopants inside of the host NC lattices.

Unlike the previously reported Mn-dopant emission, which is attributed to the Mn^{2+} d−d transition, the Cd^{2+} ion possesses fully filled frontier d-orbitals (electron configuration: $[Kr]4d^{10}$). In this case, exciting Cd^{2+} in an octahedral coordination geometry requires one electron in the e_g orbital to be transferred into a higher-energy molecular orbital. The proposed excited state of the Cd^{2+} ion and its electronic configuration are shown in Figure 4A (right panel), which is produced when one electron in the e_g orbital is lifted to the a_{1g} orbital (contributed mainly from the Cd 5s-orbital), resulting in the first excited triplet state (^3E_g). In this case, through an energy relaxation process, the Cd-PL can be assigned to the $^3E_g \rightarrow {}^1A_{1g}$ electronic transition (Figure 4A). Note that this transition is forbidden by both the Laporte and the spin selection rules,[55] consistent with the observed slow photon relaxation dynamics (1.32−1.35 ms) of the Cd-PL (Figures 2E). Furthermore, the electron paramagnetic resonance (EPR) silence of all Cd-doped samples proved that the Cd-dopant had

DOI: 10.1021/acs.jpclett.8b03412
J. Phys. Chem. Lett. 2018, 9, 7079−7084

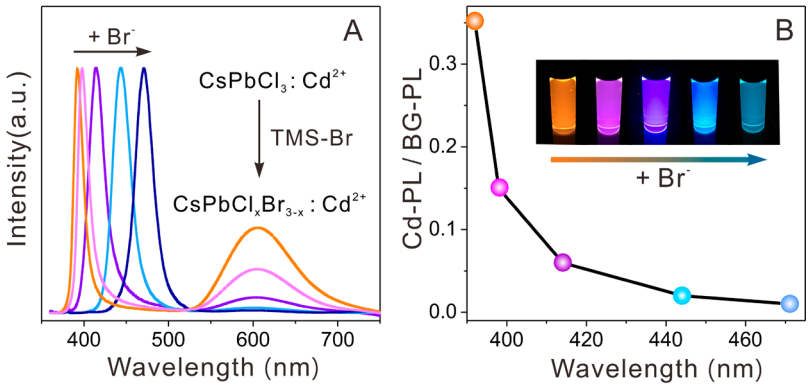

Figure 5. Evolution of (A) the PL spectrum and (B) the peak intensity ratio of Cd- to BG-PL during the ion-exchange reaction. Inset in (B): photos of the Cd-doped $CsPbCl_xBr_{3-x}$ NCs during the ion-exchange reaction.

an oxidation state of +2 (retaining the charge neutrality of the NCs) with no unpaired electrons (Figure S11), further supporting the proposed photon relaxation mechanism.

To further validate the emission mechanism and quantitatively understand the Cd-dopant emission from an energetic perspective, we performed first-principles calculations of the molecular electronic structure of $[CdCl_6]^{4-}$ within DFT using the quantum chemical ab initio software MOLPRO.[56] Because conventional DFT simulations based on the Generalized Gradient Approximation (GGA) often fail to produce accurate binding energy curves and equations of state due to the intrinsic self-interaction errors in GGA functionals, here we used hybrid density functionals that include nonlocal Hatree−Fock exchange.[57−59] The energy gap between the highest occupied molecular orbital (HOMO) and lowest unoccupied molecular orbital (LUMO) was successfully calculated for the $[CdCl_6]^{4-}$ compound (Figure 4C). At the metal−Cl bond distance range of 2.76−2.80 Å determined experimentally (Table S9), the calculated HOMO−LUMO gap fell within the range of 1.71−2.11 eV, depending on the hybrid functional employed (Figure 4C), which was in good agreement with the peak position energy of the Cd-PL (~2.03 eV). The DFT calculation results strongly supported experimental evidence that the Cd-PL originated from the electronic transition from the first excited state to the ground state of the $[CdCl_6]^{4-}$ unit in the perovskite NCs (Figure 4A).

To tailor the optical properties of Cd-doped $CsPbCl_3$ NCs, Cl-to-Br anion-exchange reactions were performed. After a controlled amount of a Br-source (i.e., bromotrimethylsilane, TMS-Br) was introduced into a Cd-doped $CsPbCl_3$ NC solution (9.28% of Cd^{2+}), the BG-PL peak red-shifted from 392 to 471 nm (Figure 5A), indicating a successful Cl-to-Br anion exchange.[12,23,24] Meanwhile, the Cd-PL became weaker and finally disappeared when the BG-PL reached 471 nm (Figure 5). This optical profile evolution can be explained by the continuous lowering of the conduction band energy of the host perovskite NCs during the Br^- ion-exchange reaction and a stationary energy level for the excited state of the Cd^{2+} ions, all of which make energy transfer from the host NCs to the Cd-dopants thermodynamically less favorable. Similar dopant emission quenching phenomena were also observed in Mn-doped perovskite NC systems.[40]

In conclusion, we describe a new category of Cd-doped perovskite NCs synthesized by decoupling the metal- and halide-precursor sources. The resulting Cd-doped NCs show dual-wavelength emission while preserving the crystal structure and morphological uniformity of the host NCs. By changing the stoichiometry of the Cd- and Pb-precursors, the $CsPbCl_3$ NCs with different Cd-doping concentrations are synthesized. We show that the new emission band originated from an energy transfer process from the photoexcited host $CsPbCl_3$ NCs to the first excited state of Cd-dopants. The subsequent electronic transition from the ^3E_g to the $^1A_{1g}$ state of the $[CdCl_6]^{4-}$ unit is responsible for the new emission feature, which is further supported by DFT calculations. Our findings make Cd-doped $CsPbCl_3$ perovskite NCs promising alternatives for doping chemistry studies in perovskites that may impact various optoelectronic applications.

■ ASSOCIATED CONTENT

Supporting Information

The Supporting Information is available free of charge on the ACS Publications website at DOI: 10.1021/acs.jpclett.8b03412.

Additional experimental and computational details, TEM images, ICP-AES data analysis, lifetime decay curves, XRD analysis of Cd-doped $CsPbCl_3$ NCs with different doping levels, and EPR spectra (PDF).

■ AUTHOR INFORMATION

Corresponding Author

*E-mail: ouchen@brown.edu.

ORCID

Hua Zhu: 0000-0003-2733-7837
Weiwei Zheng: 0000-0003-1394-1806
Brenda M. Rubenstein: 0000-0003-1643-0358
Ou Chen: 0000-0003-0551-090X

Notes

The authors declare no competing financial interest.

■ ACKNOWLEDGMENTS

O.C. acknowledges support from Brown University startup funds, the IMNI seed fund, and the National Science Foundation (OIA-1538893). O.C. also acknowledges support from the Senior Visiting Scholar Foundation of the Key Laboratory at Fudan University. O.C. thanks Eric Victor, Eunsuk Kim, and Jerome Robinson for valuable discussions. K.H.-K. is supported by the U.S. Department of Education GAANN research fellowship (P200A150037). TEM measurements were performed at the Electron Microscopy Facility in the Institute for Molecular and Nanoscale Innovation (IMNI)

DOI: 10.1021/acs.jpclett.8b03412
J. Phys. Chem. Lett. 2018, 9, 7079−7084

at Brown University. The computational parts of this research were conducted using computational resources and services at the Brown University Center for Computation and Visualization (CCV).

REFERENCES

(1) Burschka, J.; Pellet, N.; Moon, S.-J.; Humphry-Baker, R.; Gao, P.; Nazeeruddin, M. K.; Grätzel, M. Sequential deposition as a route to high-performance perovskite-sensitized solar cells. *Nature* **2013**, *499*, 316−319.
(2) Swarnkar, A.; Marshall, A. R.; Sanehira, E. M.; Chernomordik, B. D.; Moore, D. T.; Christians, J. A.; Chakrabarti, T.; Luther, J. M. Quantum dot−induced phase stabilization of α-CsPbI3 perovskite for high-efficiency photovoltaics. *Science* **2016**, *354*, 92−95.
(3) Zhu, H.; Fu, Y.; Meng, F.; Wu, X.; Gong, Z.; Ding, Q.; Gustafsson, M. V.; Trinh, M. T.; Jin, S.; Zhu, X. Y. Lead halide perovskite nanowire lasers with low lasing thresholds and high quality factors. *Nat. Mater.* **2015**, *14*, 636−642.
(4) Huang, L.; Gao, Q.; Sun, L.-D.; Dong, H.; Shi, S.; Cai, T.; Liao, Q.; Yan, C.-H. Composition-Graded Cesium Lead Halide Perovskite Nanowires with Tunable Dual-Color Lasing Performance. *Adv. Mater.* **2018**, *30*, 1800596.
(5) Han, D.; Imran, M.; Zhang, M.; Chang, S.; Wu, X.-g.; Zhang, X.; Tang, J.; Wang, M.; Ali, S.; Li, X.; Yu, G.; Han, J.; Wang, L.; Zou, B.; Zhong, H. Efficient Light-Emitting Diodes Based on in Situ Fabricated FAPbBr3 Nanocrystals: The Enhancing Role of the Ligand-Assisted Reprecipitation Process. *ACS Nano* **2018**, *12*, 8808−8816.
(6) Huang, H.; Zhao, F.; Liu, L.; Zhang, F.; Wu, X. G.; Shi, L.; Zou, B.; Pei, Q.; Zhong, H. Emulsion Synthesis of Size-Tunable CH3NH3PbBr3 Quantum Dots: An Alternative Route toward Efficient Light-Emitting Diodes. *ACS Appl. Mater. Interfaces* **2015**, *7*, 28128−28133.
(7) Xing, J.; Zhao, Y.; Askerka, M.; Quan, L. N.; Gong, X.; Zhao, W.; Zhao, J.; Tan, H.; Long, G.; Gao, L.; Yang, Z.; Voznyy, O.; Tang, J.; Lu, Z.-H.; Xiong, Q.; Sargent, E. H. Color-stable highly luminescent sky-blue perovskite light-emitting diodes. *Nat. Commun.* **2018**, *9*, 3541.
(8) Song, J.; Li, J.; Li, X.; Xu, L.; Dong, Y.; Zeng, H. Quantum Dot Light-Emitting Diodes Based on Inorganic Perovskite Cesium Lead Halides (CsPbX3). *Adv. Mater.* **2015**, *27*, 7162−7167.
(9) Li, X.; Wu, Y.; Zhang, S.; Cai, B.; Gu, Y.; Song, J.; Zeng, H. CsPbX3 Quantum Dots for Lighting and Displays: Room-Temperature Synthesis, Photoluminescence Superiorities, Underlying Origins and White Light-Emitting Diodes. *Adv. Funct. Mater.* **2016**, *26*, 2435−2445.
(10) Deng, H.; Yang, X.; Dong, D.; Li, B.; Yang, D.; Yuan, S.; Qiao, K.; Cheng, Y.-B.; Tang, J.; Song, H. Flexible and Semitransparent Organolead Triiodide Perovskite Network Photodetector Arrays with High Stability. *Nano Lett.* **2015**, *15*, 7963−7969.
(11) Ping, Y.; Zhang, J. Z. Spin-optotronic Properties of Organometal Halide Perovskites. *J. Phys. Chem. Lett.* **2018**, *9*, 6103−6111.
(12) Akkerman, Q. A.; Raino, G.; Kovalenko, M. V.; Manna, L. Genesis, challenges and opportunities for colloidal lead halide perovskite nanocrystals. *Nat. Mater.* **2018**, *17*, 394−405.
(13) Yang, H.; Zhang, Y.; Hills-Kimball, K.; Zhou, Y.; Chen, O. Building bridges between halide perovskite nanocrystals and thin-film solar cells. *Sustainable Energy & Fuels* **2018**, *2*, 2381−2397.
(14) Zhang, Q.; Yin, Y. All-Inorganic Metal Halide Perovskite Nanocrystals: Opportunities and Challenges. *ACS Cent. Sci.* **2018**, *4*, 668−679.
(15) Hills-Kimball, K.; Nagaoka, Y.; Cao, C.; Chaykovsky, E.; Chen, O. Synthesis of formamidinium lead halide perovskite nanocrystals through solid−liquid−solid cation exchange. *J. Mater. Chem. C* **2017**, *5*, 5680−5684.
(16) Zhu, H.; Cai, T.; Que, M.; Song, J. P.; Rubenstein, B. M.; Wang, Z.; Chen, O. Pressure-Induced Phase Transformation and Band-Gap Engineering of Formamidinium Lead Iodide Perovskite Nanocrystals. *J. Phys. Chem. Lett.* **2018**, *9*, 4199−4205.
(17) Protesescu, L.; Yakunin, S.; Bodnarchuk, M. I.; Krieg, F.; Caputo, R.; Hendon, C. H.; Yang, R. X.; Walsh, A.; Kovalenko, M. V. Nanocrystals of Cesium Lead Halide Perovskites (CsPbX3, X = Cl, Br, and I): Novel Optoelectronic Materials Showing Bright Emission with Wide Color Gamut. *Nano Lett.* **2015**, *15*, 3692−3696.
(18) Zhu, J.; Di, Q.; Zhao, X.; Wu, X.; Fan, X.; Li, Q.; Song, W.; Quan, Z. Facile Method for the Controllable Synthesis of CsxPbyBrz-Based Perovskites. *Inorg. Chem.* **2018**, *57*, 6206−6209.
(19) Dong, Y.; Qiao, T.; Kim, D.; Parobek, D.; Rossi, D.; Son, D. H. Precise Control of Quantum Confinement in Cesium Lead Halide Perovskite Quantum Dots via Thermodynamic Equilibrium. *Nano Lett.* **2018**, *18*, 3716−3722.
(20) Zhang, D.; Eaton, S. W.; Yu, Y.; Dou, L.; Yang, P. Solution-Phase Synthesis of Cesium Lead Halide Perovskite Nanowires. *J. Am. Chem. Soc.* **2015**, *137*, 9230−9233.
(21) Peng, L.; Dutta, A.; Xie, R.; Yang, W.; Pradhan, N. Dot−Wire−Platelet−Cube: Step Growth and Structural Transformations in CsPbBr3 Perovskite Nanocrystals. *ACS Energy Lett.* **2018**, *3*, 2014−2020.
(22) Nagaoka, Y.; Hills-Kimball, K.; Tan, R.; Li, R.; Wang, Z.; Chen, O. Nanocube Superlattices of Cesium Lead Bromide Perovskites and Pressure-Induced Phase Transformations at Atomic and Mesoscale Levels. *Adv. Mater.* **2017**, *29*, 1606666.
(23) Akkerman, Q. A.; D'Innocenzo, V.; Accornero, S.; Scarpellini, A.; Petrozza, A.; Prato, M.; Manna, L. Tuning the Optical Properties of Cesium Lead Halide Perovskite Nanocrystals by Anion Exchange Reactions. *J. Am. Chem. Soc.* **2015**, *137*, 10276−10281.
(24) Creutz, S. E.; Crites, E. N.; De Siena, M. C.; Gamelin, D. R. Anion Exchange in Cesium Lead Halide Perovskite Nanocrystals and Thin Films Using Trimethylsilyl Halide Reagents. *Chem. Mater.* **2018**, *30*, 4887−4891.
(25) Ahmed, T.; Seth, S.; Samanta, A. Boosting the Photoluminescence of CsPbX3 (X = Cl, Br, I) Perovskite Nanocrystals Covering a Wide Wavelength Range by Postsynthetic Treatment with Tetrafluoroborate Salts. *Chem. Mater.* **2018**, *30*, 3633−3637.
(26) Swarnkar, A.; Ravi, V. K.; Nag, A. Beyond Colloidal Cesium Lead Halide Perovskite Nanocrystals: Analogous Metal Halides and Doping. *ACS Energy Lett.* **2017**, *2*, 1089−1098.
(27) Swarnkar, A.; Mir, W. J.; Nag, A. Can B-Site Doping or Alloying Improve Thermal- and Phase-Stability of All-Inorganic CsPbX3 (X = Cl, Br, I) Perovskites? *ACS Energy Lett.* **2018**, *3*, 286−289.
(28) Shao, H.; Bai, X.; Cui, H.; Pan, G.; Jing, P.; Qu, S.; Zhu, J.; Zhai, Y.; Dong, B.; Song, H. White light emission in Bi3+/Mn2+ ion co-doped CsPbCl3 perovskite nanocrystals. *Nanoscale* **2018**, *10*, 1023−1029.
(29) Meinardi, F.; Akkerman, Q. A.; Bruni, F.; Park, S.; Mauri, M.; Dang, Z.; Manna, L.; Brovelli, S. Doped Halide Perovskite Nanocrystals for Reabsorption-Free Luminescent Solar Concentrators. *ACS Energy Lett.* **2017**, *2*, 2368−2377.
(30) van der Stam, W.; Geuchies, J. J.; Altantzis, T.; van den Bos, K. H.; Meeldijk, J. D.; Van Aert, S.; Bals, S.; Vanmaekelbergh, D.; de Mello Donega, C. Highly Emissive Divalent-Ion-Doped Colloidal CsPb1-xMxBr3 Perovskite Nanocrystals through Cation Exchange. *J. Am. Chem. Soc.* **2017**, *139*, 4087−4097.
(31) Yao, J.-S.; Ge, J.; Han, B.-N.; Wang, K.-H.; Yao, H.-B.; Yu, H.-L.; Li, J.-H.; Zhu, B.-S.; Song, J.-Z.; Chen, C.; Zhang, Q.; Zeng, H.-B.; Luo, Y.; Yu, S.-H. Ce3+-Doping to Modulate Photoluminescence Kinetics for Efficient CsPbBr3 Nanocrystals Based Light-Emitting Diodes. *J. Am. Chem. Soc.* **2018**, *140*, 3626−3634.
(32) Nayak, P. K.; Sendner, M.; Wenger, B.; Wang, Z.; Sharma, K.; Ramadan, A. J.; Lovrincic, R.; Pucci, A.; Madhu, P. K.; Snaith, H. J. Impact of Bi3+ Heterovalent Doping in Organic-Inorganic Metal Halide Perovskite Crystals. *J. Am. Chem. Soc.* **2018**, *140*, 574−577.
(33) Lozhkina, O. A.; Murashkina, A. A.; Shilovskikh, V. V.; Kapitonov, Y. V.; Ryabchuk, V. K.; Emeline, A. V.; Miyasaka, T. Invalidity of Band-Gap Engineering Concept for Bi3+ Heterovalent

DOI: 10.1021/acs.jpclett.8b03412
J. Phys. Chem. Lett. 2018, 9, 7079−7084

Doping in CsPbBr3 Halide Perovskite. *J. Phys. Chem. Lett.* **2018**, *9*, 5408−5411.
(34) Zou, S.; Yang, G.; Yang, T.; Zhao, D.; Gan, Z.; Chen, W.; Zhong, H.; Wen, X.; Jia, B.; Zou, B. Template-Free Synthesis of High-Yield Fe-Doped Cesium Lead Halide Perovskite Ultralong Microwires with Enhanced Two-Photon Absorption. *J. Phys. Chem. Lett.* **2018**, *9*, 4878−4885.
(35) Yong, Z. J.; Guo, S. Q.; Ma, J. P.; Zhang, J. Y.; Li, Z. Y.; Chen, Y. M.; Zhang, B. B.; Zhou, Y.; Shu, J.; Gu, J. L.; Zheng, L. R.; Bakr, O. M.; Sun, H. T. Doping-Enhanced Short-Range Order of Perovskite Nanocrystals for Near-Unity Violet Luminescence Quantum Yield. *J. Am. Chem. Soc.* **2018**, *140*, 9942−9951.
(36) Zhou, Y.; Chen, J.; Bakr, O. M.; Sun, H.-T. Metal-Doped Lead Halide Perovskites: Synthesis, Properties, and Optoelectronic Applications. *Chem. Mater.* **2018**, *30*, 6589−6613.
(37) Hassan, A.; Zhang, X.; Liu, X.; Rowland, C. E.; Jawaid, A. M.; Chattopadhyay, S.; Gulec, A.; Shamirian, A.; Zuo, X.; Klie, R. F.; Schaller, R. D.; Snee, P. T. Charge Carriers Modulate the Bonding of Semiconductor Nanoparticle Dopants As Revealed by Time-Resolved X-ray Spectroscopy. *ACS Nano* **2017**, *11*, 10070−10076.
(38) Nelson, H. D.; Li, X.; Gamelin, D. R. Computational Studies of the Electronic Structures of Copper-Doped CdSe Nanocrystals: Oxidation States, Jahn−Teller Distortions, Vibronic Bandshapes, and Singlet−Triplet Splittings. *J. Phys. Chem. C* **2016**, *120*, 5714−5723.
(39) Mondal, N.; De, A.; Samanta, A. Achieving Near-Unity Photoluminescence Efficiency for Blue-Violet-Emitting Perovskite Nanocrystals. *ACS Energy Lett.* **2019**, *4*, 32−39.
(40) Liu, W.; Lin, Q.; Li, H.; Wu, K.; Robel, I.; Pietryga, J. M.; Klimov, V. I. Mn2+-Doped Lead Halide Perovskite Nanocrystals with Dual-Color Emission Controlled by Halide Content. *J. Am. Chem. Soc.* **2016**, *138*, 14954−14961.
(41) Yuan, X.; Ji, S.; De Siena, M. C.; Fei, L.; Zhao, Z.; Wang, Y.; Li, H.; Zhao, J.; Gamelin, D. R. Photoluminescence Temperature Dependence, Dynamics, and Quantum Efficiencies in Mn2+-Doped CsPbCl3 Perovskite Nanocrystals with Varied Dopant Concentration. *Chem. Mater.* **2017**, *29*, 8003−8011.
(42) Guria, A. K.; Dutta, S. K.; Adhikari, S. D.; Pradhan, N. Doping Mn2+ in Lead Halide Perovskite Nanocrystals: Successes and Challenges. *ACS Energy Lett.* **2017**, *2*, 1014−1021.
(43) Li, Z.-J.; Hofman, E.; Davis, A. H.; Khammang, A.; Wright, J. T.; Dzikovski, B.; Meulenberg, R. W.; Zheng, W. Complete Dopant Substitution by Spinodal Decomposition in Mn-Doped Two-Dimensional CsPbCl3 Nanoplatelets. *Chem. Mater.* **2018**, *30*, 6400−6409.
(44) Parobek, D.; Dong, Y.; Qiao, T.; Son, D. H. Direct Hot-Injection Synthesis of Mn-Doped CsPbBr3 Nanocrystals. *Chem. Mater.* **2018**, *30*, 2939−2944.
(45) De, A.; Mondal, N.; Samanta, A. Luminescence tuning and exciton dynamics of Mn-doped CsPbCl3 nanocrystals. *Nanoscale* **2017**, *9*, 16722−16727.
(46) Li, F.; Xia, Z.; Pan, C.; Gong, Y.; Gu, L.; Liu, Q.; Zhang, J. Z. High Br− Content CsPb(ClyBr1−y)3 Perovskite Nanocrystals with Strong Mn2+ Emission through Diverse Cation/Anion Exchange Engineering. *ACS Appl. Mater. Interfaces* **2018**, *10*, 11739−11746.
(47) Pan, G.; Bai, X.; Yang, D.; Chen, X.; Jing, P.; Qu, S.; Zhang, L.; Zhou, D.; Zhu, J.; Xu, W.; Dong, B.; Song, H. Doping Lanthanide into Perovskite Nanocrystals: Highly Improved and Expanded Optical Properties. *Nano Lett.* **2017**, *17*, 8005−8011.
(48) Milstein, T. J.; Kroupa, D. M.; Gamelin, D. R. Picosecond Quantum Cutting Generates Photoluminescence Quantum Yields Over 100% in Ytterbium-Doped CsPbCl3 Nanocrystals. *Nano Lett.* **2018**, *18*, 3792−3799.
(49) Zhou, D.; Liu, D.; Pan, G.; Chen, X.; Li, D.; Xu, W.; Bai, X.; Song, H. Cerium and Ytterbium Codoped Halide Perovskite Quantum Dots: A Novel and Efficient Downconverter for Improving the Performance of Silicon Solar Cells. *Adv. Mater.* **2017**, *29*, 1704149.
(50) Kroupa, D. M.; Roh, J. Y.; Milstein, T. J.; Creutz, S. E.; Gamelin, D. R. Quantum-Cutting Ytterbium-Doped CsPb(Cl1−xBrx)3 Perovskite Thin Films with Photoluminescence Quantum Yields over 190%. *ACS Energy Lett.* **2018**, *3*, 2390−2395.
(51) Zhang, X.; Zhang, Y.; Zhang, X.; Yin, W.; Wang, Y.; Wang, H.; Lu, M.; Li, Z.; Gu, Z.; Yu, W. W. Yb3+ and Yb3+/Er3+ doping for near-infrared emission and improved stability of CsPbCl3 nanocrystals. *J. Mater. Chem. C* **2018**, *6*, 10101−10105.
(52) Imran, M.; Caligiuri, V.; Wang, M.; Goldoni, L.; Prato, M.; Krahne, R.; De Trizio, L.; Manna, L. Benzoyl Halides as Alternative Precursors for the Colloidal Synthesis of Lead-Based Halide Perovskite Nanocrystals. *J. Am. Chem. Soc.* **2018**, *140*, 2656−2664.
(53) Yang, Y.; Chen, O.; Angerhofer, A.; Cao, Y. C. On Doping CdS/ZnS Core/Shell Nanocrystals with Mn. *J. Am. Chem. Soc.* **2008**, *130*, 15649−15661.
(54) Cottrell, T. L. *Dynamic Aspects of Molecular Energy States*; Wiley: New York, 1965.
(55) Atkins, P. W. In *Molecular Quantum Mechanics*, 5th ed.; Friedman, R., Ed.; Oxford University Press: Oxford, 2011.
(56) Werner, H.-J.; Knowles, P. J.; Knizia, G.; Manby, F. R.; Schütz, M. Molpro: a general-purpose quantum chemistry program package. *Wiley Interdisciplinary Reviews: Computational Molecular Science* **2012**, *2*, 242−253.
(57) Adamo, C.; Barone, V. Toward reliable density functional methods without adjustable parameters: The PBE0 model. *J. Chem. Phys.* **1999**, *110*, 6158−6170.
(58) Zhao, Y.; Schultz, N. E.; Truhlar, D. G. Exchange-correlation functional with broad accuracy for metallic and nonmetallic compounds, kinetics, and noncovalent interactions. *J. Chem. Phys.* **2005**, *123*, 161103.
(59) Zhao, Y.; Truhlar, D. G. The M06 suite of density functionals for main group thermochemistry, thermochemical kinetics, noncovalent interactions, excited states, and transition elements: two new functionals and systematic testing of four M06-class functionals and 12 other functionals. *Theor. Chem. Acc.* **2008**, *120*, 215−241.

DOI: 10.1021/acs.jpclett.8b03412
J. Phys. Chem. Lett. 2018, 9, 7079−7084